

Full length article

Idarubicin-loaded biodegradable microspheres enhance sensitivity to anti-PD1 immunotherapy in transcatheter arterial chemoembolization of hepatocellular carcinoma



Zhiying Zheng^{a,b,1}, Mingxi Ma^{c,1}, Xiuping Han^{d,1}, Xiao Li^{e,1}, Jinxin Huang^c, Yuetong Zhao^d, Hanyuan Liu^e, Junwei Kang^b, Xiangyi Kong^a, Guoqiang Sun^e, Guangshun Sun^e, Jie Kong^{f,*}, Weiwei Tang^{a,*}, Guoqiang Shao^{d,*}, Fei Xiong^{c,*}, Jinhua Song^{a,*}

^a Hepatobiliary Center, Key Laboratory of Liver Transplantation, Chinese Academy of Medical Sciences, NHC Key Laboratory of Living Donor Liver Transplantation, The First Affiliated Hospital of Nanjing Medical University, Nanjing, China

^b Department of Anesthesiology and Perioperative Medicine, The First Affiliated Hospital of Nanjing Medical University, Nanjing, China

^c State Key Laboratory of Bioelectronics, Jiangsu Key Laboratory for Biomaterials and Devices, School of Biological Science and Medical Engineering & Collaborative Innovation Center of Suzhou Nano-Science and Technology, Southeast University, Nanjing, China

^d Department of Nuclear Medicine, Nanjing First Hospital, Nanjing Medical University, Nanjing, China

^e Department of General Surgery, Nanjing First Hospital, Nanjing Medical University, Nanjing, China

^f Department of Intervention, Nanjing First Hospital, Nanjing Medical University, Nanjing, China

ARTICLE INFO

Article history:

Received 21 May 2022

Revised 23 November 2022

Accepted 2 December 2022

Available online 10 December 2022

Keywords:

Idarubicin
Hepatocellular carcinoma
Transcatheter arterial chemoembolization
Biodegradable microspheres
Immune
PD-L1
PDI

ABSTRACT

Transarterial chemoembolization (TACE) is an image-guided locoregional therapy used for the treatment of patients with primary hepatocellular carcinoma (HCC). However, conventional TACE formulations such as epirubicin-lipiodol emulsion are rapidly dissociated due to the instability of the emulsion, resulting in insufficient local drug concentrations in the target tumor. To overcome these limitations, we used biodegradable Idarubicin loaded microspheres (BILMs), which were prepared from gelatin and carageenan and could be loaded with Idarubicin (IDA-MS). The morphology and the ability to load and release IDA of BILMs were characterized *in vitro*. We evaluated tumor changes and side effects after TACE treatment with IDA-MS in VX2 rabbit and C57BL/6 mice HCC models. In addition, the effect of IDA-MS on the tumor immune microenvironment of HCC tumors was elucidated via mass spectrometry and immunohistochemistry. Result showed that IDA-MS was developed as a new TACE formulation to overcome the poor delivery of drugs due to rapid elimination of the anticancer drug into the systemic circulation. We demonstrated in rabbits and mice HCC models that TACE with IDA-MS resulted in significant tumor shrinkage and no more severe adverse events than those observed in the IDA group. TACE with IDA-MS could also significantly enhance the sensitivity of anti-PD1 immunotherapy, improve the expression of CD8⁺ T cells, and activate the tumor immune microenvironment in HCC. This study provides a new approach for TACE therapy and immunotherapy and illuminates the future of HCC treatment.

Statement of significance

Conventional transarterial chemoembolization (TACE) formulations are rapidly dissociated due to the instability of the emulsion, resulting in insufficient local drug concentrations in hepatocellular carcinoma (HCC). To overcome these limitations, we used biodegradable microspheres called BILMs, which could be loaded with Idarubicin (IDA-MS). We demonstrated in rabbits and mice HCC models that TACE with IDA-MS resulted in significant tumor shrinkage and no more severe adverse events than those observed in the IDA group. TACE with IDA-MS could also significantly enhance the sensitivity of anti-PD1 immunotherapy,

* Corresponding authors.

E-mail addresses: kilogram@163.com (J. Kong), 1243773473twww@sina.com (W. Tang), guoqiangshao@163.com (G. Shao), xiongfei@seu.edu.cn (F. Xiong), jinhuasongnanji@163.com (J. Song).

¹ Indicates all are first authors

improve the expression of CD8⁺ T cells, and activate the tumor immune microenvironment in HCC. This study provides a new approach for TACE therapy and immunotherapy and illuminates the future of HCC treatment.

© 2022 The Author(s). Published by Elsevier Ltd on behalf of Acta Materialia Inc.
This is an open access article under the CC BY-NC-ND license
(<http://creativecommons.org/licenses/by-nc-nd/4.0/>)

1. Introduction

Liver cancer is a malignant tumor arising from hepatocytes or intrahepatic bile duct epithelial cells, with insidious onset, rapid progression and poor prognosis [1]. According to the latest statistics, in 2020, there will be 748,300 new cases of liver cancer and 695,900 deaths from liver cancer worldwide [2]. Half of these new cases and deaths occurred in China, which has one of the highest rates of liver cancer in East Asia [3]. When diagnosed early and when the tumor is <5 cm in size, liver transplantation and surgical resection are the treatment option for hepatocellular carcinoma (HCC), as the most common liver cancer. However, a majority of the patients present at advanced stages because the disease is mostly asymptomatic in early stages [4].

Image-guided intra-arterial therapy, such as transarterial chemoembolization (TACE), is a valuable tool in the treatment of primary HCC [5]. The infusion emulsion such as epirubicin-lipiodol emulsion delivers anticancer drugs directly to the tumor and blocks terminal arterioles with lipiodol [6,7]. However, the clinical outcomes of TACE remain unsatisfactory, typically causing a partial response in only 15–55% of patients and increasing median survival from 16 to 20 months [8,9]. During TACE surgery, due to the instability of the emulsion, a considerable part of chemotherapy drugs enter the systemic circulation, resulting in low administration efficiency and systemic side effects. Therefore, the establishment of a new TACE drug delivery system that facilitates drug delivery is crucial to enhance tumor control and reduce the side effects of HCC.

Cancer cells including HCC are capable of evading immune surveillance, facilitating cancer development via activating diverse immunity checkpoint signal paths. Monoclonal antibodies that target immunity checkpoints have witnessed a huge breakthrough in tumor treatment, promoting the immunity-mediated eradication of oncocytes. Amongst those, programmed death-ligand 1 (PD-L1)/programmed death 1(PD1) and Cytotoxic T-Lymphocyte Antigen (CTLA)-4 suppressors have already been utilized in some malignant cancers, but molecules that are capable of disrupting other co-suppressive signal paths are under exploration, like T cell immune globulin and T cell immunoglobulin and immune-receptor tyrosine-based inhibitory motif domain (TIGIT), lymphocyte activation gene-3 (LAG3), and T cell immunoglobulin containing the mucin domain 3 (TIM3). In the era of immune therapy, immune checkpoint inhibitors (ICIs) have been examined for HCC sufferers as well, especially, nivolumab and pembrolizumab have been accepted for second line treatment [10]. Nevertheless, resembling other gastric intestinal malignant cancers, the HCC responsive rate of ICIs as a mono therapy is low, hence new combined methods involving TACE [11,12], tyrosine kinase inhibitors (TKIs) [13], and other medicines are being investigated intensively at present.

Idarubicin (IDA) is an antineoplastic drug commonly used to treat hematologic diseases. Due to their relative lipophilic properties and a longer biological half-life, this anthracycline is also used in TACE as part of HCC therapy [14]. However, conventional TACE formulations such as epirubicin-lipiodol emulsion are rapidly dissociated due to the instability of the emulsion, resulting in insufficient local drug concentrations in the target tumor. Drug eluting

microbeads (DEBs) are the next generation embolic agent products of the lipiodol emulsion. They can penetrate into tumor blood vessels and release chemotherapeutic in a controlled and sustained manner [15]. Most of them are size-calibrated microspheres, typically composed of artificial polymer hydrogel, and able to block blood flow permanently. In fact, various matrix materials give microspheres different functions, such as radiopacity and absorbability. Self-visualized radiopaque microbeads would offer direct intraprocedural visual feedback regarding TACE treatment localization [16]. They could be prepared by incorporating metal elements [17] or linking iodine species to polymer chains [18,19]. To avoid long-term chronic inflammation and facilitate potential repeated treatments, biodegradable DEBs were developed [20]. For example, Okamoto et al. synthesized Lipiodol/ polycaprolactone (PCL) beads using microfluidics and air-plasma treatment, which could simultaneously release miriplatin [21]. It is worth mentioning that natural polymers are promising materials for preparing DEBs. Gelatin is a natural polymer with good biocompatibility and degradability, which has been used clinically as an embolic agent for decades [22]. Carrageenan is a polysaccharide rich in sulfate groups extracted from algae. Carrageenan has good gel ability and many biological activities, such as antibacterial, anticancer, and antiviral [23]. At present, it has been widely used in tissue engineering, regenerative medicine, and three-dimension(3D) bioprinting [24–26]. And the sulfated groups can rely on electrostatic adsorption to let carrageenan carry a variety of drugs, including IDA.

In the present study, we used biodegradable Idarubicin loaded microspheres (BILMs), which were prepared from gelatin and carrageenan and could be loaded with IDA (IDA-MS). The morphology and the ability to load and release IDA of BILMs were characterized in vitro. In addition, we demonstrated in rabbits and mice HCC models that TACE with IDA-MS resulted in significant tumor shrinkage and no more severe adverse events than those observed in the IDA group. TACE with IDA-MS could also significantly enhance the sensitivity of anti-PD1 immunotherapy, improve the expression of CD8⁺ T cells, and activate the tumor immune microenvironment in HCC. This study provides a new approach for TACE therapy and immunotherapy and illuminates the future of HCC treatment.

2. Materials and methods

2.1. Preparation of BILMs

Carrageenan and gelatin were brought from Aladdin Industrial Corporation. Liquid paraffin, Span 80, and isopropanol were purchased from Sinopharm Chemical Reagent Co., Ltd. Glutaraldehyde (ca. 50% in water) were purchased from TCI Shanghai and IDA(hydrochloride form) was purchased from Nanjing Chia-Tai Tianqing Pharmaceutical Co., Ltd. The preparation of BILMs used the emulsifying cross-linking method previously reported by Liu et al. [27]. In short, 2160 mg of carrageenan and 840 mg of gelatin were fully mixed in 50 ml of deionised water at 70 °C to form the water phase. 150 ml of liquid paraffin was mixed with 375 µl Span80 to form the oil phase. Water phase and oil phase were evenly mixed by a mechanical agitator (RW 20 digital, IKA) with 400 rpm. After maintaining 70 °C for 30 min, the whole system

was immediately immersed in iced water for 30 min and cooled to about 4 °C. Subsequently, glutaraldehyde was added to the system and the dose reached 0.15% (V/V). In the whole process, the rotating speed of the mechanical mixer is maintained at 400 rpm. Finally, the solidified microspheres were recovered from the oil phase with isopropanol. The final samples were obtained after being placed in a vacuum dryer for three days.

2.2. IDA loading efficiency

In this experiment, the standard curve of idarubicin concentration and optical density (OD) at 490 nm was established by using an enzyme labeling instrument (SUNRISE, TECAN) [28]. Briefly, 10 mg of idarubicin was mixed evenly with water and fixed to 5 ml to obtain a solution with a concentration of 2 mg/ml. 50 µg/ml IDA were prepared by taking 25 µl of the solution and diluted to 1 ml. Then six different concentrations of IDA were obtained (50, 25, 12.5, 6.25, 3.125 and 1.5625 µg/ml). Take 200 µl of each of the six samples, place them in a 96 well plate, and measure their OD at 490 nm. Subsequently, the function between OD and IDA concentration was established.

250 µl idarubicin aqueous solution (2 mg/ml) was added to BILMs with a volume of 100 µL after swelling [29,30]. The diameter of microspheres is 100–300 µm after swelling. The BILMs and IDA were mixed evenly by shaking the container gently. Then, the microspheres and the remaining IDA solution were separated after 5 min, 10 min, 15 min, 30 min, 1 h, and 2 h. A 29 G syringe was used to separate the supernatant and microspheres. In order to collect all the IDA not carried by the microspheres, the microspheres were washed with 500 µl deionised water. The supernatant and the water for washing are collected together and the volume is fixed to 2 ml. 200 µl of each IDA supernatant sample was taken and measured at 490 nm and their concentration can be calculated by the function established above. Three parallel samples were set at each time point. So, the IDA loading efficiency at each time point can be obtained by the following formula:

$$\text{Loading efficiency}(\%) = \frac{\text{initial IDA mass} - \text{the concentration of the remaining solution} \times \text{volume}(2\text{ml})}{\text{initial IDA mass}} \times 100\%$$

2.3. Morphology, size, and distribution

About 4 mg microspheres were soaked in water and placed on glass slides, and their appearance was observed with an optical microscope (Eclipse E200, Nikon). 200 microspheres were selected randomly and their diameters were recorded. Then a few BILMs in 2.2 mixed with IDA solution after 30 min were observed and recorded in the same way.

2.4. The release of IDA in vitro

500 µl 2 mg/ml of idarubicin was added to 200 µl BILMs. After loading the drug for 30 min, the microspheres were separated from the supernatant and soaked into 40 ml 0.9% NaCl saline solution [29]. The whole system is placed in a constant temperature shaker (THZ-312, Shanghai Jinghong Experimental Equipment Co., Ltd) with a temperature of 37 °C and a speed of 100 r/min. 500 µl soaking solution was taken out at the time points of 15 min, 30 min, 1 h, 3 h, 6 h, 12 h, 24 h, 72 h, and 96 h, and 500 µl fresh saline solution was added to maintain the total volume. The same methods were used to measure the concentration of IDA in the soaking solution. The standard curve of OD and concentration of IDA in 0.9% NaCl saline solution was established. All operations are the same as in 2.2 except for changing water into 0.9% NaCl saline solution. Thus, the cumulative drug release in the soaking solution at each time point can be calculated. There were three parallel samples.

2.5. Cell cultures

The mouse HCC cell line H22 and rabbit HCC cell line VX2 were obtained from the Cell Bank of Type Culture Collection (Chinese Academy of Sciences, China). H22 and VX2 cells were cultured in RIPA 1640 medium (Gibco, USA) containing 10% FBS, 50 U. mL⁻¹ penicillin (Thermo Fisher Scientific, USA), and 50 mg. mL⁻¹ streptomycin (Thermo Fisher Scientific, USA). The maintenance was conducted on overall cell lines under the temperature of 37 °C within one constant-temperature incubator covering 5% CO₂.

2.6. Preparation of preclinical rabbit liver tumor model

The animal experiment was approved by the Animal Management Committee of Nanjing Medical University, and all experimental procedures and animal care followed the institutional ethics guidelines for animal-related experiments. Male New Zealand white rabbits weighing 3.0–3.5 kg. The animals were housed in experimental animal-specific cages on a 12-hour light/dark cycle. Before all manipulations, animals were injected intramuscularly with 5 mg/kg body weight of thiamine-zolazepam (Zoletil 50, Virbac, Carros, France) and 2 mg/kg body weight of 2% xylazine hydrochloride (Rompun; Bayer, Seoul, South Korea). Throughout the study, the VX2 carcinoma strain was maintained in the right hindlimb of vector rabbits by deep intramuscular injection. The left lobe of the animal's liver was surgically exposed, and a small piece of fresh tumor tissue was removed from the tumor and implanted directly into the subcapsular area of the liver of each rabbit. Tumors were incubated for 17–18 days prior to treatment.

2.7. Rabbit liver tumor model grouping and drug delivery

The animals were randomly divided into 2 groups with similar tumor volumes: animals treated with an intra-arterial (IA)

infusion of IDA solution (IDA group, n = 3) and IDA-MS solution (IDA-MS group, n = 3). The dose of IDA-MS injected into liver tumor tissue was 0.5 mg. During IA delivery, a 4-French catheter (VER angiographic catheter, Cordis, USA) was inserted into the right central artery for arterial access. To access the correct hepatic artery, advance the a 2.7-Fr(French) microcatheter (Progreat Micro Catheter system, Terumo, Japan) through the catheter into the descending aorta. After hepatic arteriography was performed to confirm tumor staining and reveal the correct hepatic artery, microcatheterization was selectively performed until the catheter tip was gently placed adjacent to the proper hepatic artery. The mixture(mixtures of IDA-MS microspheres and contrast agent) prepared for each group was then gently applied under fluoroscopic guidance. After the mixture is completely injected, the microcatheter is withdrawn and the puncture site is carefully squeezed to stop the bleeding. Digital subtraction angiography (DSA) and positron emission tomography-computer tomography (PET-CT) were recorded before and after TACE treatment.

2.8. In vivo tumor mice model and treatment

20 Male C57BL/6 mice (5, 6 weeks old) were purchased from and bred under specific pathogen-free (SPF) conditions at the Nanjing Medical University Laboratory Animal Center. The mice were euthanized by cervical dislocation.

To establish a subcutaneous tumor-bearing mouse model, 2×10^6 H22 cells mixed in 100 μ l PBS were subcutaneously inoculated into the right axillary region of C57BL/6 mice. After that, every 5 mice were randomly assigned to one group. Different groups were as follows: IDA, IDA-MS, IDA+ α PD1, and IDA-MS+ α PD1. When the tumors grew into 80–150 mm³ in volume, IDA/IDA-MS (4 mg kg⁻¹, once a week) was intratumoral injected into the mice in different groups. From the second day of injection, 200ug anti-mouse-PD1(α PD1; BE0273; Bio X Cell, USA) were injected intraperitoneally into the mice in IDA+ α PD1 and IDA-MS+ α PD1 groups twice a week. The tumor size was measured every 3 days and the tumor volume was calculated using the following formula: volume (mm³) = width² × length/2.

2.9. Hematoxylin-eosin (HE) and immunohistochemistry

The HCC mouse model specimens were taken, embedded in paraffin, sectioned to 4 mm thickness, and subjected to HE staining

$$\text{Loading efficiency}(\%) = \frac{500\mu\text{g} - [(OD + 0.007095) \div 0.009281]\mu\text{g/ml} \times 2\text{ml}}{500\mu\text{g}} \times 100\%$$

and immunohistochemistry according to the protocol. The dUTP-biotin nick end labeling (TUNEL) staining method in the samples used DAB (SA-HRP) TUNEL apoptosis detection kit (Servicebio, China), in 0.01 mol L⁻¹ citrate buffer (pH 6.0; Wobixin Inc., China). Samples were blocked in PBS with 2% BSA for 1 hour at ambient temperature and were treated with monoclonal antibodies to CD3 (ab16669, 1:150 dilution; Abcam, UK), CD8 (ab217344, 1:2000 dilution; Abcam, Cambridge, UK), Ki-67 (ab16667, 1:2000 dilution; Abcam, Cambridge, UK) and PD-L1 (ab213524, 1:250 dilution; Abcam, UK), followed by enzyme-conjugated secondary antibody (ab6721, 1:1000 dilution; Abcam, UK) for 1 hour at ambient temperature. Detection was performed the next day with 3'-diaminobenzidine according to the manufacturer's instructions. Images were acquired using a laser scanning confocal microscope (Zeiss, Germany).

2.10. Mass cytometry

We obtained tissue samples from the IDA and IDA-MS tumor-bearing groups. We then processed mouse tumor tissue using the Miltenyi Mouse Tumor Isolation Kit (Miltenyi Biotec, Germany), in which Percoll removes debris and divides red blood cells. CyTOF staining includes the following steps: 194Pt staining → Fc block staining → surface antibody staining → overnight DNA staining (191/193Ir) → intracellular antibody staining → computer acquisition of data. Data analysis steps include FlowJo preprocessing (loop and select single, live, intact CD45⁺ immune cells), bioinformatics analysis (X-shift algorithm performs cell subpopulation clustering, manual annotation, TSNE dimensionality reduction visual display, and statistical analysis). This experiment was carried out in PLT-TECH Company (Plttech, China).

2.11. Statistical analysis

Statistical analyses were carried out using the GraphPad Prism 9.0 (GraphPad software Inc., USA), and two-tailed *P* value < 0.05 was considered to be statistically significant. An independent *t*-test was used to compare the continuous variables between the two groups.

3. Results

3.1. The loading efficiency of IDA

The properties of embolic microspheres play a decisive role in the therapeutic effect of TACE. BILMs prepared from carageenan and gelatin were used. Carrageenan, the main component, could carry a variety of drugs through ion exchange mechanism. In our previous research, we have confirmed that BILMs have excellent mechanical properties, customizable size, and the ability to load and controllable release of Doxorubicin [27]. In this study, we characterized the interaction between BILMs and Idarubicin.

Firstly, the standard curve between the concentration of IDA aqueous solution and the OD at 490 nm was established (Fig. 1A).

The drugs unloaded by BILMs existed in the remaining IDA solution. The concentration of the residual solution can be calculated by measuring the optical density and using the standard curve in Fig. 1A. The IDA loading efficiency was calculated as follows:

As shown in Fig. 1B, the loading efficiency of 0.1 ml BILMs for 500 μ g IDA could exceed 99% within 10 min. The effective drug loading amount of IDA was defined as 5 mg/ml microspheres. The loading efficiency reached 99.12% at 5 min, which indicated that BILMs have a good ability to carry IDA. In addition, Table 1 is listed to compare the various properties of BILMs and several commercial embolic agents [22,27–29,31]. Commercially available drug-eluting microspheres are usually composed of biocompatible synthetic polymers which cause permanent embolism. For example, the main components of DC BeadTM and CallisSphere[®] are PVA. However, HCC recurs frequently and requires repeated treatment [32]. The residue of non-degradable microspheres at the lesion will lead to difficulties in subsequent embolization by occupying the route for catheterization [33]. Unlike other drug-eluting microspheres, BILMs are composed of bioabsorbable and biocompatible natural polymers. BILMs will degrade after causing intravascular embolism for a sufficient period of time, leaving space for subsequent operations.

3.2. Morphology, size, and distribution of BILMs

The morphology and proper diameter distribution of microspheres is very important for catheter delivery and adequate vascular embolization. Therefore, it is necessary to study the effect of drug loading on the size and shape of BILMs [22]. An optical microscope was used to observe the morphology of BILMs before and after begin loading with IDA. It can be seen that BILMs are light yellow microspheres (Fig. 1C-a). After absorbing IDA, they turned into red-orange and maintained the same shape (Fig. 1C-b).

The size and distribution of BILMs(100–300 μ m) in two states were also statistically analyzed. It can be seen from Fig. 1D that the size range of BILMs before and after loading IDA are basically the same. More than 99% of the microspheres are in the range of 150 ~ 290 μ m. However, the average diameter of BILMs with IDA decreased from 212.15 μ m to 196.55 μ m. This is due to a 17% increase in the proportion of microspheres smaller than 200 μ m.

3.3. The release of IDA in vitro

Similarly, the standard curve of IDA concentration in 0.9% NaCl solution and OD was established (Fig. 1E). The cumulative release of IDA in the soaking solution at each time point can be obtained

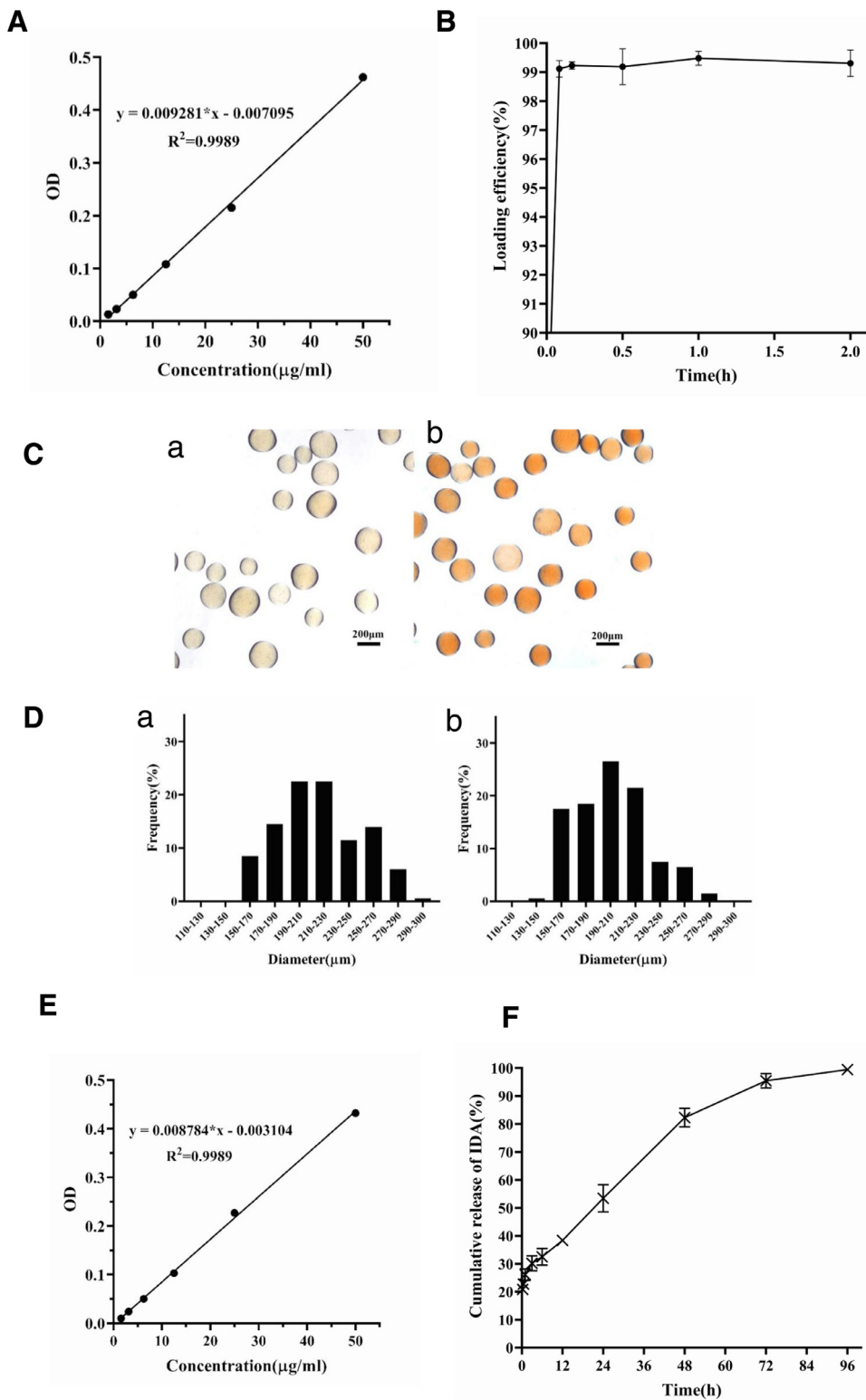


Fig. 1. IDA Loading efficiency, morphology and release of IDA in vitro. (A) Standard curve of the concentration of idarubicin in water and the OD at 490 nm. The function is $y = 0.009281 \times x - 0.007095$. (B) IDA Loading efficiency of BILMs($n = 3$). The ratio of IDA to BILMs is 5 mg/ml. (C) The morphology of BILMs before(a) and after(b) loaded with IDA. (D)Diameter distribution of BILMs before(a) and after(b) loaded with IDA. Random 200 microspheres were counted in each group. (E) Standard curve of the concentration of idarubicin in 0.9% NaCl solution and the OD at 490 nm. The function is $y = 0.008784 \times x - 0.003104$. (F) Cumulative release of IDA in 0.9% NaCl saline solution.

Table 1
Summary of IDA-loaded microspheres.

Trade names	Material	Diameter(μm)	Loading times (5 mg of IDA per 1 ml of microsphere) [†]	Absorbable(Y/N)
BILMs	Carrageenan and gelatin	30–1200 ²⁷	5min	Yes
DC Bead™	Polyvinyl alcohol-co-Poly(2-acrylamido-2-methylpropane sulfonate) ²²	70–500	15 min ²⁸	No
CalliSphere®	Chemical modified polyvinyl alcohol (PVA)	100–1200	10 min ²⁹	No
HepaSphere™	Polyvinyl acetate-co-poly(methylacrylate) ²²	30–100	30 min ²⁸	No
TANDEM ®	Sodium methacrylate hydrogel ³¹	40, 75, 100	15 min ²⁸	No
LifePearl™	Copolymer of polyethylene glycol diacrylamide	100–400	15 min ²⁸	Unknown

[†] The loading efficiency should be above 95%.

by measuring the concentration of IDA in the soaking solution [34]. The cumulative release of IDA (%) was calculated as follows:

$$\text{Cumulative release of IDA}(\%) = \frac{\text{the cumulative release of IDA in soaking solution at each time point}}{\text{initial IDA mass}} \times 100\% = \frac{\frac{[(OD+0.003104)-0.008784]\mu\text{g}}{\text{ml}} \times 40\text{ml} + x}{1000\mu\text{g}} \times 100\%$$

$$x = 0.5\text{ml} * (\text{IDA concentration at } 15\text{min} + \text{IDA concentration at } 30\text{min} + \dots)$$

It should be noted that the drug aliquot used to analysis contains drugs, so x in the formula represents the total content of IDA in the soaking solution taken for detection before each time point. Fig. 1F showed the drug release rate of 0.2 ml BILMs loaded with about 1 mg IDA in normal saline. The bursting release of IDA was observed and the release rate reached 38.4% in 12 h. The data reached 53.43% after 24 h and the release rate exceeded 95% after 72 h.

3.4. TACE with IDA-MS significantly inhibited tumor growth in rabbit VX2 HCC model

We established the rabbit VX2 HCC model using 6 rabbits, 3 for IDA-MS and 3 for IDA. As shown in Fig. 2A, DSA results showed that TACE with IDA-MS blocked blood vessels more obviously than the IDA group. Transverse section in PET-CT images before TACE and 7 days after TACE in IDA and IDA-MS group revealed that IDA-MS group showed higher tumor reduction than the IDA group (Fig. 2B). Coronal section median sagittal section and metabolic region of rabbits' PET-CT images before TACE and 7 days after TACE in IDA and IDA-MS group also confirmed the same results (Fig. 3A).

In order to evaluate the effects of TACE with IDA-MS on tumor tissues, paracancer tissues and other important organs, we used HE staining to confirm that compared with the IDA group, TACE with IDA-MS reduced tumor infiltration, but no more severe damage to the heart, liver, spleen, lung, and kidney (Fig. 3B).

3.5. TACE with IDA-MS reduced tumor growth and increased the efficiency of anti-PD1 treatment in mice HCC model

To further examine the correlation between IDA-MS and the growth of HCC *in vivo*, we respectively injected H22 cells with IDA, IDA-MS, IDA+αPD1, and IDA-MS+αPD1 groups into C57BL/6 mice subcutaneously, and then carried out PD1 mAb injection to assess their anti-tumor capability. More details about the experimental scheme of xenograft mice model were listed in Fig. 4A. According to the results, compared with IDA group, the volume and weight of the tumor decreased significantly after IDA-MS injection. Compared with IDA+αPD1 group, IDA-MS+αPD1 quite decreased the tumor weight and volume (Fig. 4B–4D). PET results revealed that compared with IDA group, the concentration of the tumor decreased significantly after IDA-MS injection. Compared with

IDA+αPD1 group, IDA-MS+αPD1 quite decreased the tumor concentration (Fig. 4E–4F).

By HE staining, we confirmed the tumor tissue and morphologic changes in different groups. Compared with the IDA-MS group, the cells in the IDA group were more disorganized, with enlarged stained nuclei and less cytoplasmic content. In the IDA-MS+αPD1 group, tumor cells were arranged more regularly than in the previous three groups (Fig. 5A). Given the immunohistochemical results, Ki67 expression in IDA-MS group significantly decreased compared with IDA group, and the decline was noticeably facilitated under the combination with PD1 mAb (Fig. 5A–5B). The expression of TUNEL expression was just the opposite, in line with the expected results (Fig. 5A–5B). However, the expression of CD3, CD8 and PD-L1 moderately increased after IDA-MS injection compared with IDA (Fig. 5A–5B). With the combined use of PD1 mAb in IDA+αPD1 and IDA-MS+αPD1 group, the expression of CD8 was further increased, while PD-L1 was decreased (Fig. 5A–5B). Accordingly, this study revealed injection of IDA-MS was capable of inducing apoptosis, reducing tumor growth, and enhancing the efficiency of PD1 mAb treatment in a xenograft HCC mice model *in vivo*.

3.6. Changes of tumor immune microenvironment after IDA-MS treatment in HCC mice model based on mass cytometry

To further assess the overall immune microenvironment variations of the HCC tumors in IDA group and IDA-MS group, we used mass cytometry to measure the expression of the respective immune cell clusters. We cycled single, live, and intact CD45⁺ immune cells from the selected cells in the respective tissues. All samples showed clustering and subgroup annotation of CD45⁺ immune cells. The results showed that CD45⁺ immune cells was increased in IDA-MS group compared to IDA group (Fig. 6A–6B). There were 29 cell clusters in total, and we defined the respective cell cluster based on the specific markers of the respective cell type (Figs. 6C–6D, 7).

CD4⁺T cells, CD8⁺ T cells, natural killer (NK) cells, monocytes increased whereas macrophages decreased after IDA-MS injection compared with IDA group (Fig. 6E). Additionally, we assessed the overall expression of PD-L1(CD274), PD1(CD279), and cytokines (IFN-γ, TNF-α) in the immune microenvironment. According to the results, after the injection of IDA-MS, the expression of PD-L1 and IFN-γ, TNF-α increased (Fig. 8B–8E). But PD1 showed no difference

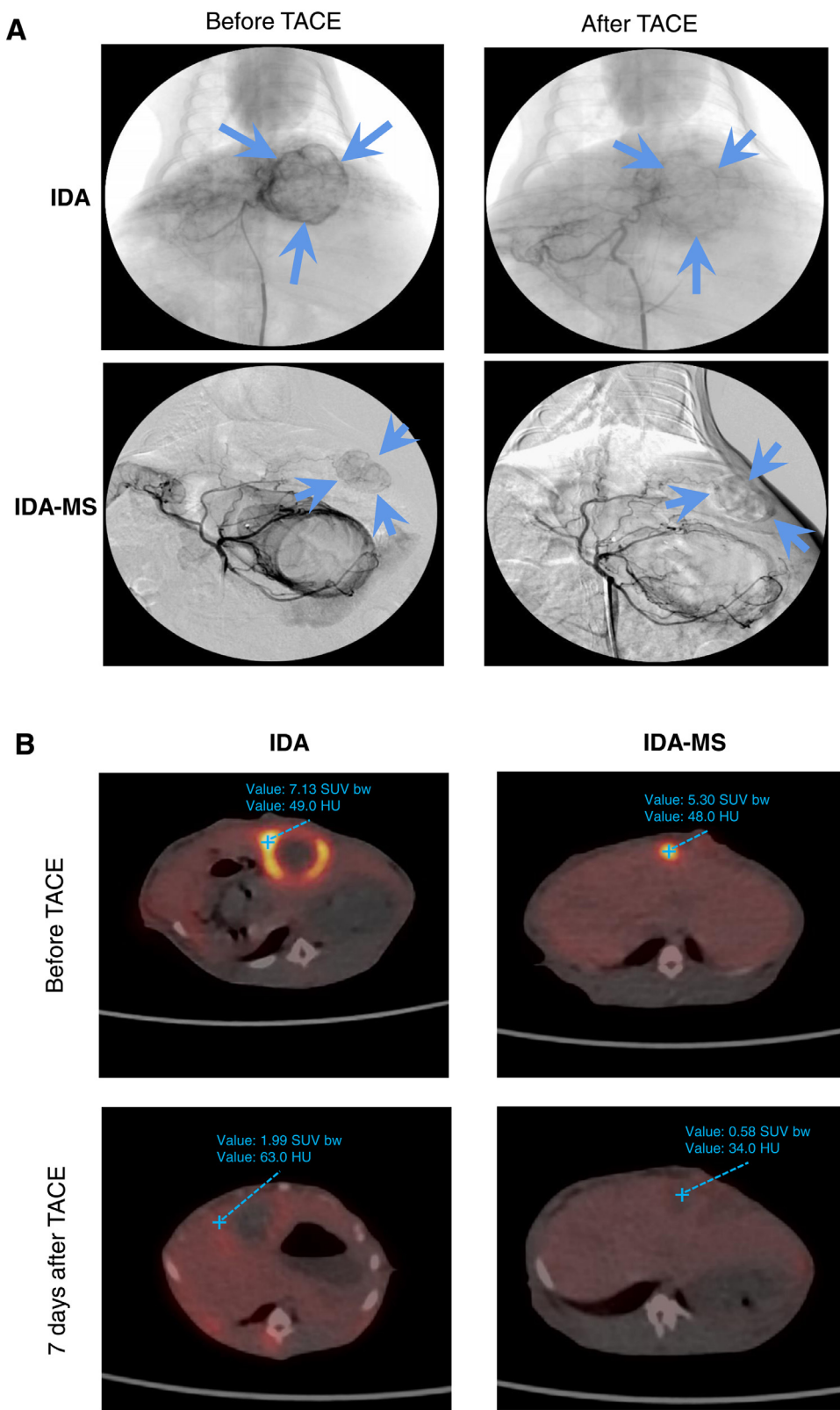


Fig. 2. The results of DSA and PET-CT after TACE with IDA-MS or IDA in VX2 rabbit liver model. (A) Real-time DSA of pre- and post-embolizing in IDA and IDA-MS group. (B) Transverse section in PET-CT images before TACE and 7 days after TACE in IDA and IDA-MS group.

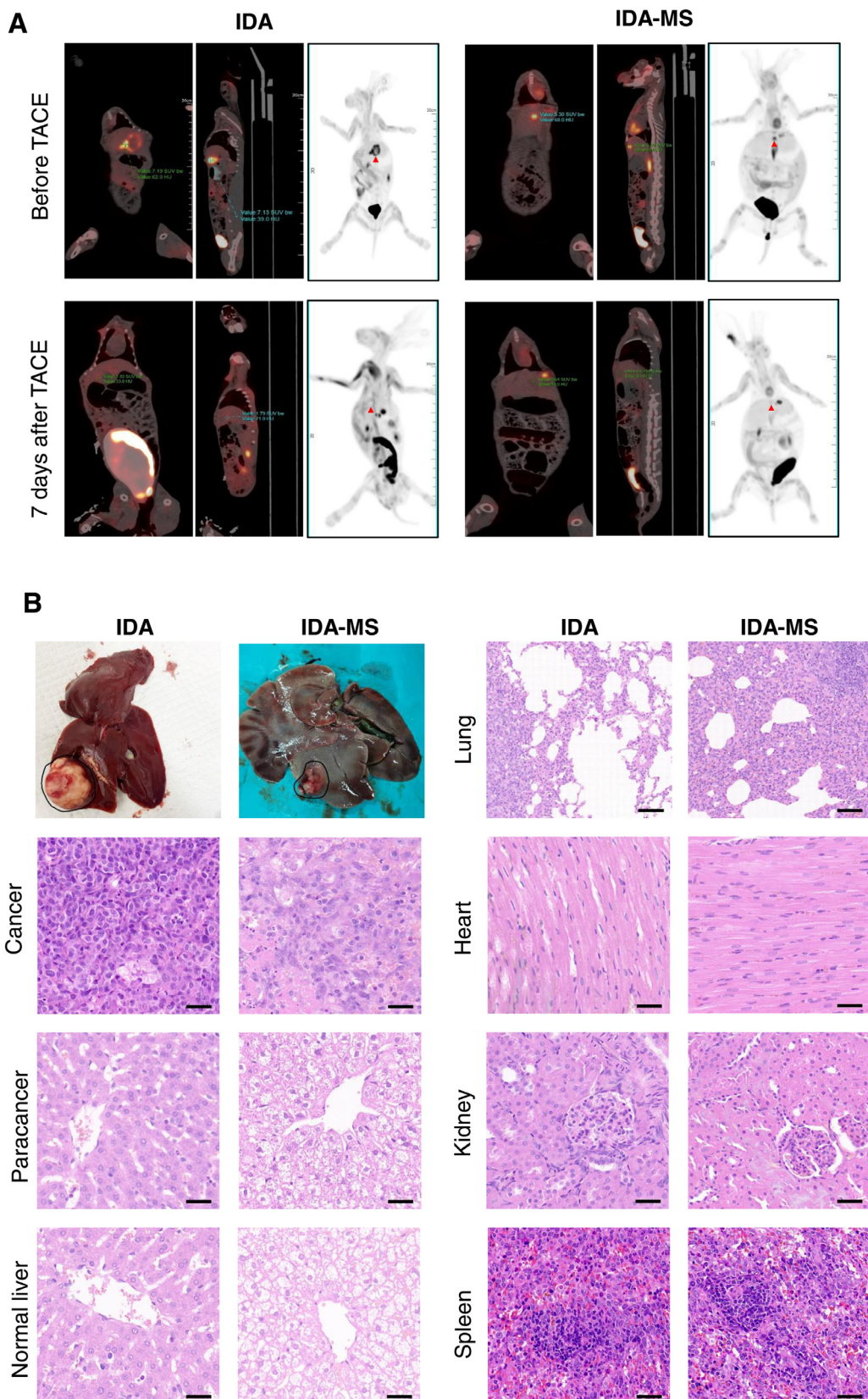


Fig. 3. The results of PET-CT and HE staining after TACE with IDA-MS or IDA in VX2 rabbit liver model. (A) Coronal section median sagittal section and metabolic region of rabbits' PET-CT images before TACE and 7 days after TACE in IDA and IDA-MS group. (B) Overview of organ tumor and HE staining picture of respective organs or tissues. Scale bar: 25 μ m.

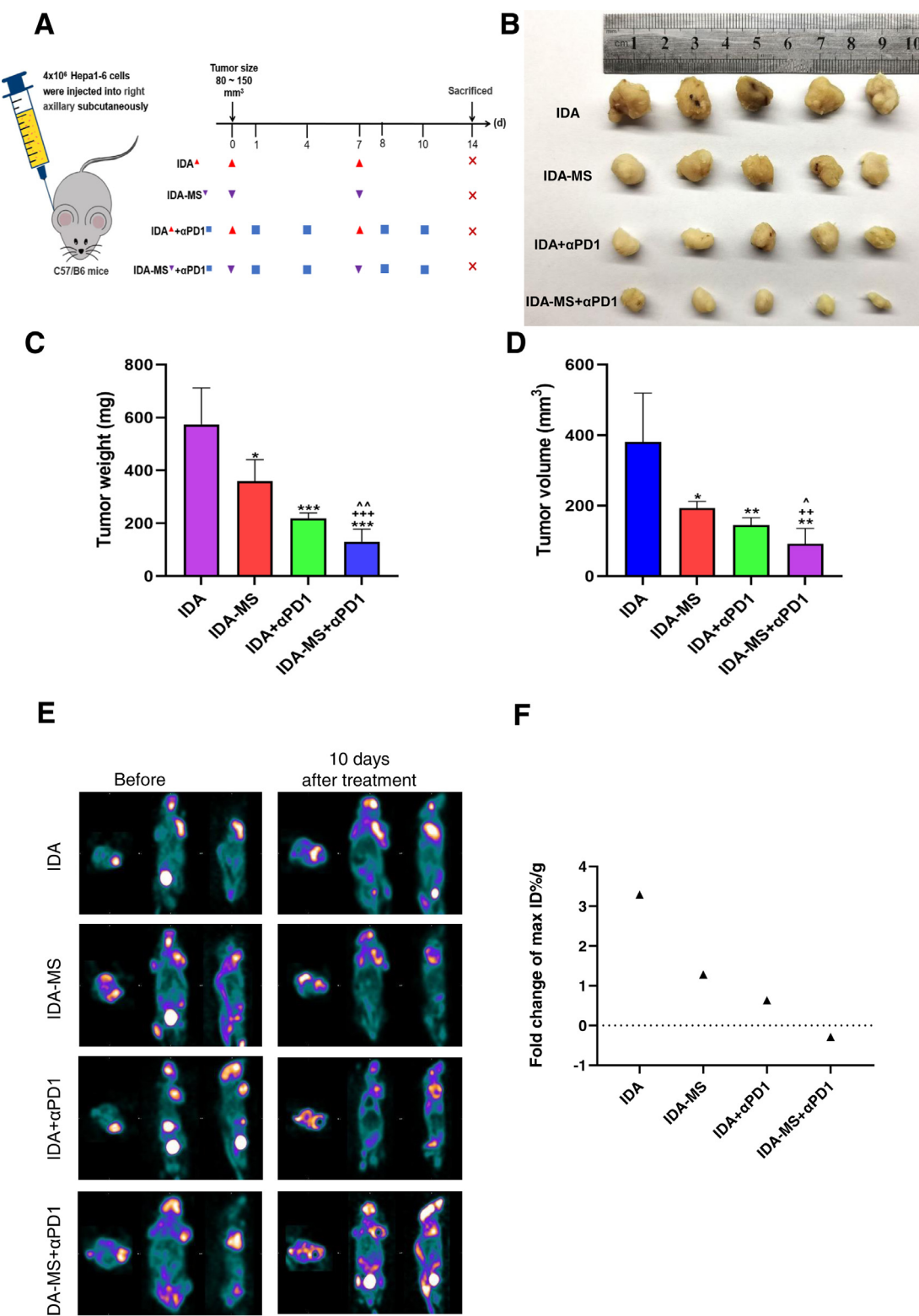


Fig. 4. IDA-MS reduced tumor growth and increased the efficiency of anti-PD1 in H22 tumor model. (A) Experimental design. (B) Photographs of excised tumors in each group (IDA, IDA-MS, IDA+ α PD1, and IDA-MS+ α PD1). (C-D) The volume (C) and weight (D) statistics of subcutaneous tumors in the respective group. (E) PET images for each group of tumor-bearing rats. (F) Fold change of max ID%/g.

(Fig. 8A, 8E). The above results show that injection of IDA-MS could lead to the increase of PD-L1 on the surface of cancer cells, creating a tumor immune microenvironment that is conducive to the effect of PD1 mAb in HCC.

4. Discussion

TACE is often the first choice for the treatment of intermediate-stage HCC and as a bridge-therapy for liver transplantation. Drug-

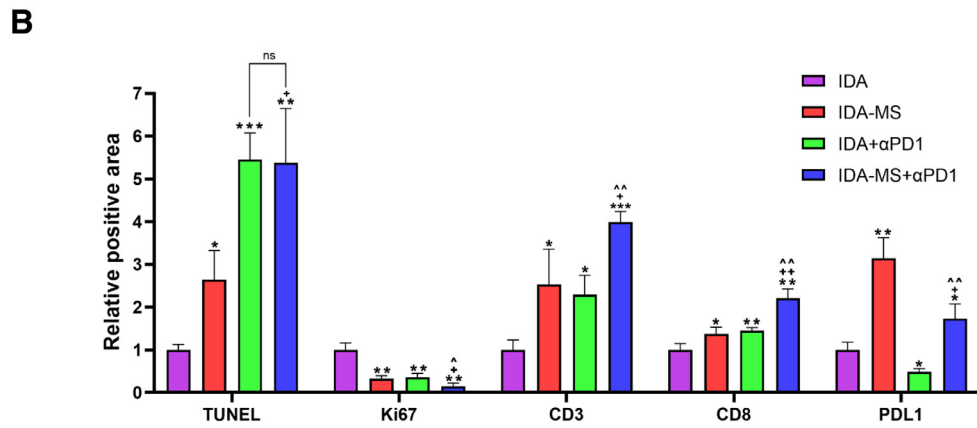
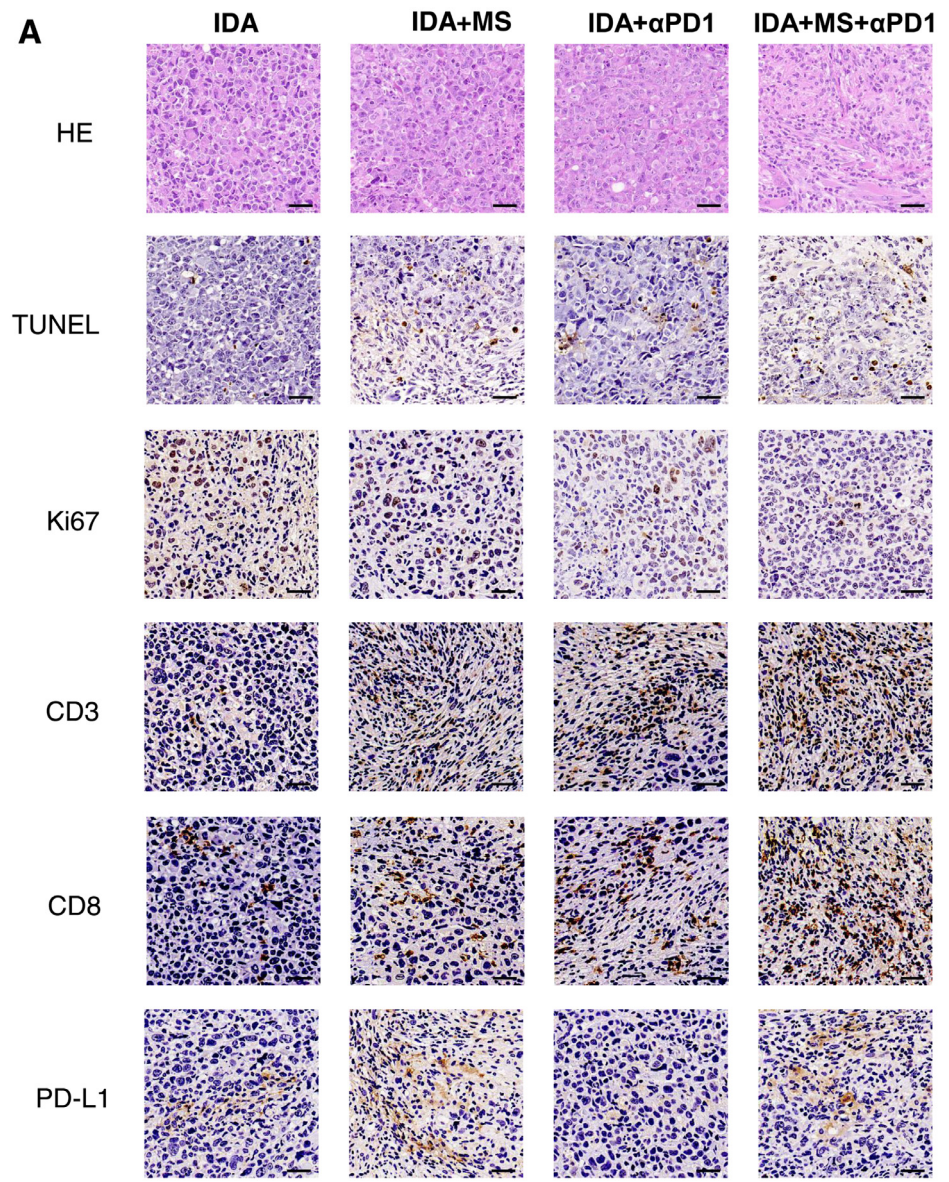


Fig. 5. HE and immunohistochemical results after TACE with IDA-MS or IDA in H22 tumor model. (A) Immunohistochemistry of tumor sections in each group. The morphology of subcutaneous tumors in four groups was confirmed by HE staining. Moreover, the upper panel also indicates immunohistochemical results of Ki67, TUNEL, PD-L1, CD3, and CD8 expression in each group. Scale bar: 25 μ m (B) The results of corresponding indicator statistics in four groups. **P < 0.01 vs IDA group; ***P < 0.001 vs IDA group +P < 0.05 vs IDA-MS group; ++P < 0.01 vs IDA-MS group ^P < 0.05 vs IDA-MS+ α PD1 group; ^^P < 0.01 vs IDA-MS+ α PD1 group.

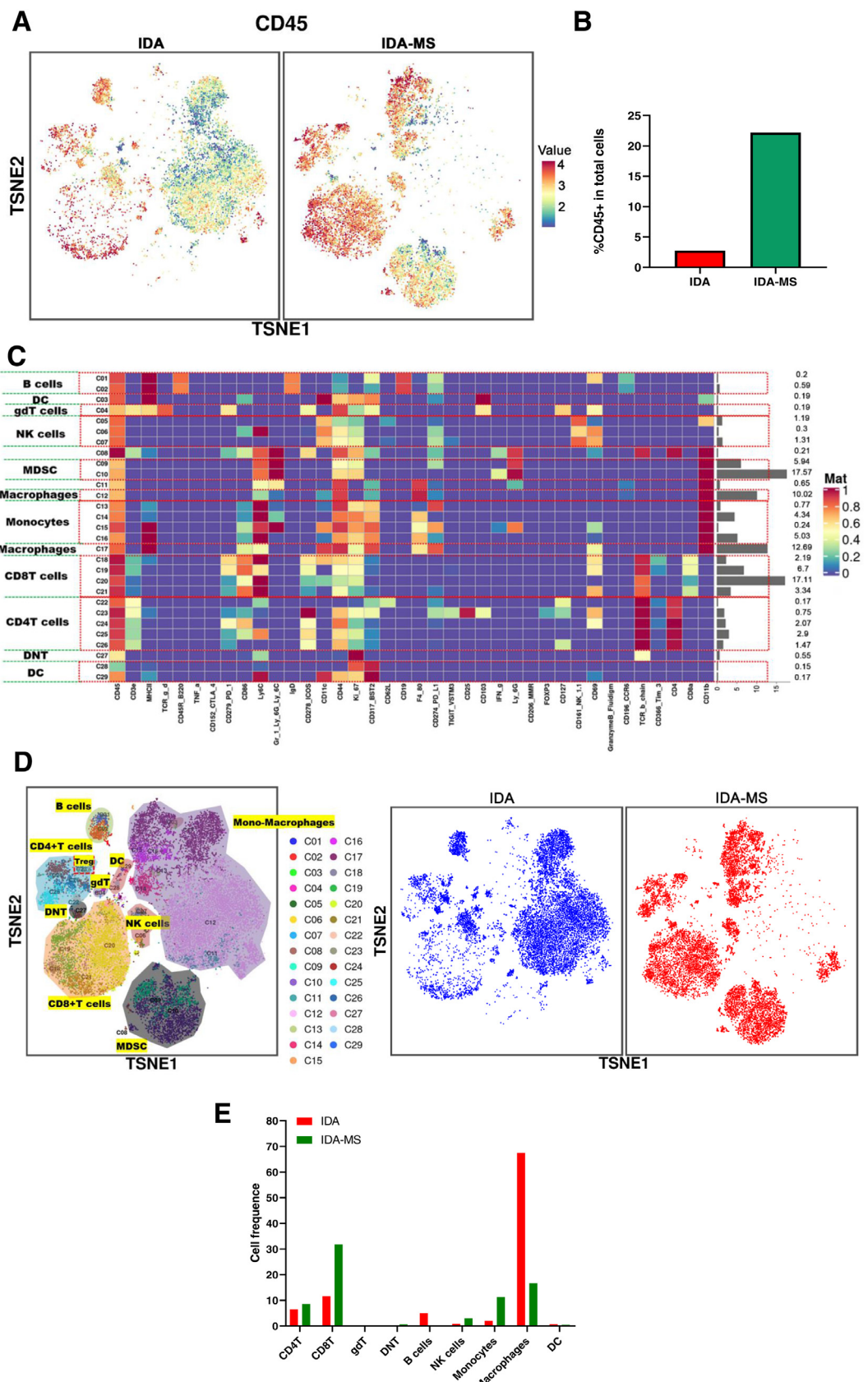


Fig. 6. Mass cytometry reflected the immune microenvironment of subcutaneous H22 tumors after IDA/IDA-MS treatment. (A) Distribution of CD45⁺ cells by t-SNE plot. (B) The ratio of CD45⁺ cells in the IDA and IDA-MS group respectively. (C) A total of 29 cell clusters were divided, and we defined the respective group. (D) t-SNE plot showing distributions of 29 cell clusters and the t-SNE diagram showing the distribution of cell clusters in the respective sample. (E) The histogram showing the number of the respective cell cluster in different groups by mass cytometry.

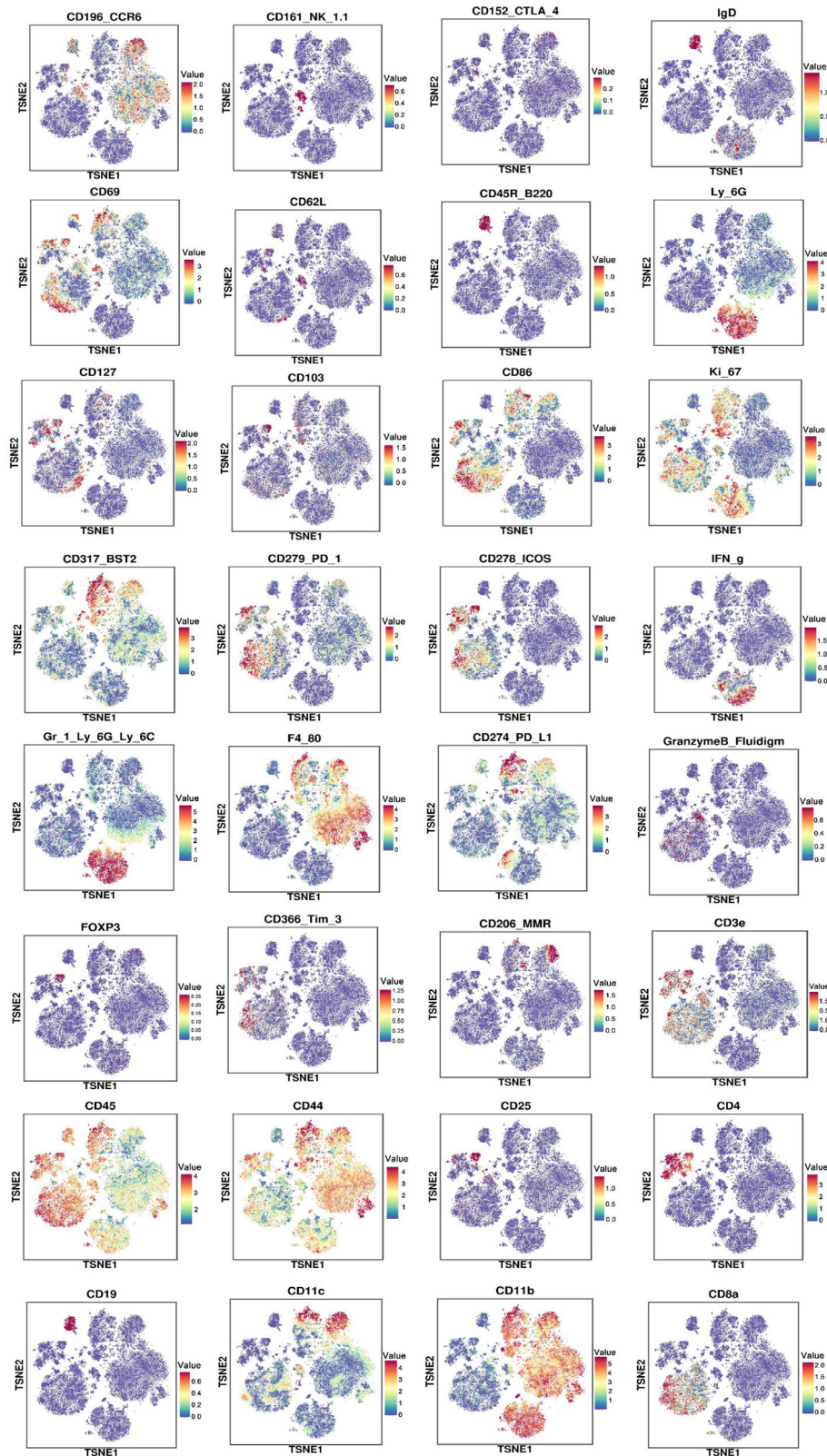


Fig. 7. The expression of cell clustering marker genes via mass cytometry. TSNE as a form of presentation.

eluting bead-TACE(DEB-TACE) is more effective and easier to tolerate than conventional TACE [35,36]. DEBs are non-absorbable embolic microspheres that can be loaded with cytotoxic agents, which were developed to achieve more sustained drug release with embolization [37,38]. The positively charged protonated amine

groups present in doxorubicin and idarubicin can interact with the negatively charged sulfonates of the microspheres, which are loaded [39]. Despite no priority evidence, doxorubicin was the most commonly used drug for DEB-TACE [40]. It has been shown that the time to HCC progression was significantly better in

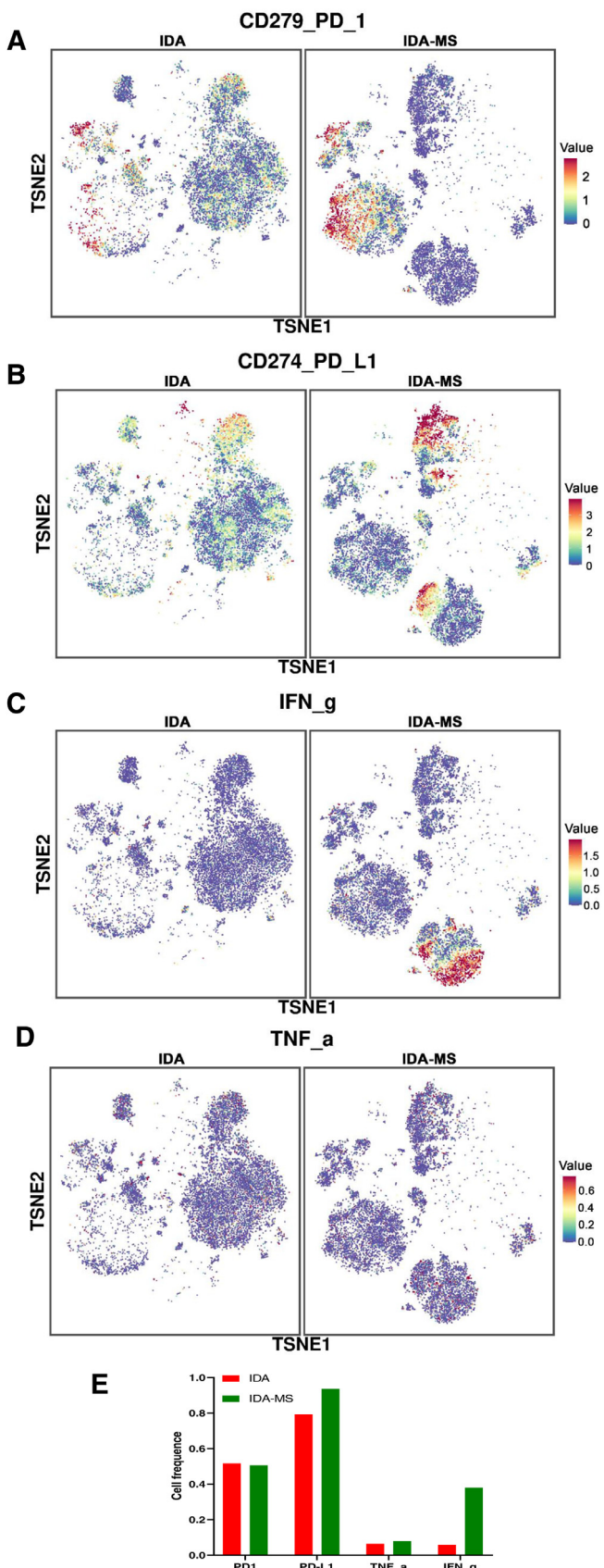


Fig. 8. Mass cytometry reflected the marker expression changes after IDA/IDA-MS treatment. (A–D) TSNE plot showing the distribution of PD1, PD-L1, IFN-g and TNF-a in subcutaneous H22 tumors in the IDA and IDA-MS groups. (E) The histogram showing the number of PD1⁺ cells, PD-L1⁺ cells, IFN-g⁺ cells, and TNF-a⁺ cells cluster in IDA and IDA-MS groups.

the doxorubicin-DEB-TACE(DOX-DEB-TACE) group than in the TACE group (11.7 vs. 7.6 months) and that DEB-TACE therapy led to better treatment outcomes in intermediate stage HCC [35]. Although DOX being most commonly administered, there are no universally accepted treatment protocols in DEB-TACE, and recent studies have suggested many other drug regimens [41]. For example, DOX and radioactive species, such as iodine-131 (¹³¹I) or rhenium-188 (¹⁸⁸Re), are attached to the microspheres matrix to achieve the combination of TACE and transarterial radioembolization (TARE) and produce a synergistic antitumor effect [42,43]. Some studies have loaded newer anti-tumor drugs into DEBs. Denys et al. studied *in vivo* pharmacokinetics, safety and toxicity evaluation of vandetanib eluting beads using swine liver embolization model [44]. Sahr et al. successfully loaded anti-VEGF antibodies onto the embolic microspheres and the controlled release of the drug was confirmed *in vitro* [45].

More and more preclinical and early clinical studies have shown that, also as an anthracycline, IDA seems to have more advantages than doxorubicin in antitumor efficacy and safety. In an *in vitro* study of the cytotoxicity of anticancer drugs on three human hepatoma cells, idarubicin showed the most active anticancer effect compared with doxorubicin and 9 other common chemotherapeutic drugs [39]. Furthermore, with reference to doxorubicin in rapid infusion, the relative cardiotoxicity of idarubicin was 0.53, and idarubicin required less therapeutic dose [46]. A multicenter, prospective, single-arm, phase II clinical trial reported a 6-month objective response rate of 52% in patients with advanced HCC in the study using idarubicin-DEBs (IDA-DEBs) for TACE, and median overall survival was 18.6 months [30]. In addition, this study had a lower incidence of treatment discontinuation (9% vs 29%) compared to doxorubicin-eluting beads plus placebo arm of the sorafenib or placebo plus TACE trial [47]. Also, the majority of grade 3–4 TACE-related adverse events in subjects with IDA-DEB-TACE were biological/transient without any sequelae [30].

Small diameter beads have been shown to cause total necrosis of the target lesion because smaller diameter beads can be embolized more distally and thus block collateral channels [35], but 40 μm microspheres may be more toxic due to the dependent of size compared to 100 μm microspheres [48]. In this study, diameter of the 99% microspheres used in loading IDA is 150 ~ 290 μm, and the IDA-MS was promising to be developed as a new TACE formulation to overcome the poor delivery of drugs due to rapid elimination of the anticancer drug into the systemic circulation.

In addition, we demonstrated in rabbits and mice HCC models that TACE with IDA-MS resulted in tumor shrinkage and no more severe adverse events than those observed in the IDA group. In the rabbit experiment, IDA also showed noteworthy anti-tumor effect even without loaded microspheres, which may be due to the high lipophilicity of IDA, resulting in higher cell penetration of lipid membrane and more drug accumulation in lipiodol, which eventually exerted anti-tumor effects [49,50]. In the murine model, we validated the anti-tumor efficacy by subcutaneous intratumoral injection. However, in experiments with mice, we found that IDA alone did not seem to demonstrate such a powerful cancer-inhibiting effect after intratumoral injection into rat subcutaneous tumors. This may be due to that the intratumorally injected IDA was metabolized too quickly and failed to exert cytotoxicity in a sustained manner. Furthermore, we found that the anti-cancer efficacy in the IDA-MS group was increased compared with the IDA group, which may have confirmed this view from another aspect.

In this study, we firstly demonstrated that intratumoral injection of IDA-MS would contribute to enhancing the sensitivity of anti-PD1 immunotherapy, improve the expression of CD8⁺ T cells, and activate the tumor immune microenvironment in HCC. It has been reported blocking PD1/PD-L1, nivolumab [51] and camrelizumab [52], indicated the substantial anti-tumor effect on pa-

tients with advanced HCC [51–53], which brought new solutions to HCC treatment. However, in clinical practice, a considerable number of patients had no response to anti-PD1 immunotherapy and develop drug resistance. The expression of PD-L1 could be used as a predictor of anti-PD1 immunotherapy, and lack of PD-L1 expression was an important mechanism of resistance to anti-PD1/PD-L1 therapies [54]. In this study, in contrast to the depletion of PD-L1 expression in the IDA group, the expression of PD-L1 was significantly increased after the intratumoral injection of IDA-loaded microspheres, which led to immune activation. Moreover, in this study, mass cytometry was used to more comprehensively analyze changes in the tumor microenvironment. The newly synthesized IDA-MS in our study not only increased the expression of PD-L1 in the tumor, but also increased the expression of CD8⁺ T cells, NK cells and IFN- γ , and these interventions jointly promoted the activation of immune function. It opened up a new regimen for anti-PD1 immunotherapy in cancer.

Our experiments also have some limitations. Firstly, we failed to simulate IDA-MS enhancing PD1/PD-L1 blockade therapy in the rabbit liver cancer model due to the failure to find the PD1 mAb against rabbits. Secondly, mass cytometry cannot eliminate the heterogeneous information of tumor cells, and more accurate sequencing techniques such as single-cell sequencing should be used for specific cell population sequencing analyses. Thirdly, we still need to further explore the mechanism by which intratumoral injection of IDA-MS led to the marked elevation of PD-L1. At last, our study is mainly limited to animal experiments, and further clinical trials are needed to verify the reliability of the conclusions of this study.

5. Conclusion

In summary, the present study reveals that the IDA-MS is developed as a new TACE formulation to overcome the poor delivery of drugs due to rapid elimination of the anticancer drug into the systemic circulation. TACE with IDA-MS resulted in tumor shrinkage and no more severe adverse events than those observed in the IDA group. TACE with IDA-MS could also enhance the sensitivity of anti-PD1 immunotherapy, improve the expression of CD8⁺ T cells, and activate the tumor immune microenvironment in HCC. This study provides a new approach for TACE therapy and immunotherapy and illuminates the future of HCC treatment.

Funding

This work was supported by the grants from National Key Research and Development Program of China (Grant No.2017YFA0205501), the National Natural Science Foundation of China (Grant No.82073804).

Details of authors' contributions

4 first authors were listed in this manuscript. Dr. ZYZ, MXM, XPH and XL were responsible for designing the study, performing part of the experiments, as well as drafting the manuscript. Furthermore, we have 5 corresponding authors in this manuscript. Dr. JHS, FX, GGS, WWT and JK have contributed to the study design, data interpretation, editing, and critical revision of the manuscript. Other authors also contributed to performing part of the experiments, and data interpretation. All authors read and approved the final manuscript.

Declaration of Competing Interest

The authors declare that they have no competing interests.

Acknowledgments

None.

References

- [1] V. Treska, J. Bruha, V. Liska, J. Fichtl, K. Prochazkova, T. Petrakova, P. Hosek, Pros and cons of portal vein embolization with hematopoietic stem cells application in colorectal liver metastases surgery, *In Vivo* 34 (5) (2020) 2919–2925 (Brooklyn) Sep-Oct.
- [2] Y. Collin, A. Paré, A. Belblidia, R. Létourneau, M. Plasse, M. Dagenais, S. Turcotte, G. Martel, A. Roy, R. Lapointe, F. Vandenbroucke-Menu, Portal vein embolization does not affect the long-term survival and risk of cancer recurrence among colorectal liver metastases patients: a prospective cohort study, *Int. J. Surg.* 61 (2019) 42–47 Jan.
- [3] D.C. Madoff, B.C. Odisio, E. Schadde, R.C. Gaba, R.J. Bennink, T.M. van Gulik, B. Guiu, Improving the safety of major resection for hepatobiliary malignancy: portal vein embolization and recent innovations in liver regeneration strategies, *Curr. Oncol. Rep.* 22 (6) (2020) 59 May 16.
- [4] E. Chakraborty, D. Sarkar, Emerging therapies for hepatocellular carcinoma (HCC), *Cancers* 14 (11) (2022) 2798 (Basel) Jun 4.
- [5] J. Willatt, K.K. Hannawa, J.A. Ruma, T.L. Frankel, D. Owen, P.M. Barman, Image-guided therapies in the treatment of hepatocellular carcinoma: a multidisciplinary perspective, *World J. Hepatol.* 7 (2) (2015) 235–244 Feb 27.
- [6] R.C. Gaba, R. Emmadi, A. Parvinian, L.C. Casablanca, Correlation of doxorubicin delivery and tumor necrosis after drug-eluting bead transarterial chemoembolization of rabbit VX2 liver tumors, *Radiology* 280 (3) (2016) 752–761 Sep.
- [7] J.M.M. van Breugel, J.F. Geschwind, S. Mirpour, L.J. Savic, X. Zhang, R. Duran, M. Lin, M. Miszczyk, E. Liapi, J. Chapiro, Theranostic application of lipiodol for transarterial chemoembolization in a VX2 rabbit liver tumor model, *Theranostics* 9 (13) (2019) 3674–3686 May 27.
- [8] J.M. Llovet, J. Bruix, Systematic review of randomized trials for unresectable hepatocellular carcinoma: chemoembolization improves survival, *Hepatology* 37 (2) (2003) 429–442 Feb.
- [9] W. Ma, J. Jia, S. Wang, W. Bai, J. Yi, M. Bai, Z. Quan, Z. Yin, D. Fan, J. Wang, G. Han, The prognostic value of 18F-FDG PET/CT for hepatocellular carcinoma treated with transarterial chemoembolization (TACE), *Theranostics* 4 (7) (2014) 736–744 May 1.
- [10] V. Longo, A. Gnoni, A. Casadei Gardini, S. Pisconti, A. Licchetta, M. Scartozzi, R. Memeo, V.O. Palmieri, G. Aprile, D. Santini, P. Nardulli, N. Silvestris, O. Brunetti, Immunotherapeutic approaches for hepatocellular carcinoma, *Oncotherapy* 8 (20) (2017) 33897–33910 May 16.
- [11] O.B. Gbolahan, M.A. Schacht, E.W. Beckley, T.P. LaRoche, B.H. O’Neil, M. Pyko, Locoregional and systemic therapy for hepatocellular carcinoma, *J. Gastrointest Oncol.* 8 (2) (2017) 215–228 Apr.
- [12] A.S. Mikhail, M. Mauda-Havakuk, A.H. Negussie, N. Hong, N.M. Hawken, C.J. Carlson, J.W. Owen, O. Franco-Mahecha, P.G. Wakim, A.L. Lewis, W.F. Pritchard, J.W. Karanian, B.J. Wood, Evaluation of immune-modulating drugs for use in drug-eluting microsphere transarterial embolization, *Int. J. Pharm.* 616 (2022) 121466 Mar 25.
- [13] H. Li, C.W. Li, X. Li, Q. Ding, L. Guo, S. Liu, C. Liu, C.C. Lai, J.M. Hsu, Q. Dong, W. Xia, J.L. Hsu, H. Yamaguchi, Y. Du, Y.J. Lai, X. Sun, P.B. Koller, Q. Ye, M.C. Hung, MET inhibitors promote liver tumor evasion of the immune response by stabilizing PDL1, *Gastroenterology* 156 (6) (2019) 1849–1861 May 13.
- [14] B. Bourcier, F. Lagarce, V. Lebreton, Stability of a high-concentrated aqueous solution of idarubicin stored in a polypropylene syringe for transarterial chemoembolization, *J. Pharm. Biomed. Anal.* 210 (2022) 114543 Feb 20.
- [15] A.L. Lewis, S.L. Willis, M.R. Dreher, Y. Tang, K. Ashrafi, B.J. Wood, E.B. Levy, K.V. Sharma, A.H. Negussie, A.S. Mikhail, Bench-to-clinic development of imageable drug-eluting embolization beads: finding the balance, *Future Oncol.* 14 (26) (2018) 2741–2760 Nov.
- [16] A.S. Mikhail, W.F. Pritchard, A.H. Negussie, G. Inkiyad, D.J. Long, M. Mauda-Havakuk, P.G. Wakim, W. van der Sterren, E.B. Levy, A.L. Lewis, J.W. Karanian, B.J. Wood, Cone-beam computed tomography-based spatial prediction of drug dose after transarterial chemoembolization using radiopaque drug-eluting beads in woodchuck hepatocellular carcinoma, *Invest Radiol.* 57 (8) (2022) 495–501 Aug 1.
- [17] A.H. Negussie, Q.M.B. de Ruiter, H. Britton, D.R. Donahue, Q. Boffi, Y.S. Kim, W.F. Pritchard, C. Moonen, G. Storm, A.L. Lewis, B.J. Wood, Synthesis, characterization, and imaging of radiopaque bismuth beads for image-guided transarterial embolization, *Sci. Rep.* 11 (1) (2021) 533 Jan 12.
- [18] R. Duran, K. Sharma, M.R. Dreher, K. Ashrafi, S. Mirpour, M. Lin, R.E. Scherthaner, T.R. Schlachter, V. Tacher, A.L. Lewis, S. Willis, M. den Hartog, A. Radaelli, A.H. Negussie, B.J. Wood, J.F. Geschwind, A novel inherently radiopaque bead for transarterial embolization to treat liver cancer - a pre-clinical study, *Theranostics* 6 (1) (2016) 28–39 Jan 1.
- [19] K. Ashrafi, Y. Tang, H. Britton, O. Domene, D. Blino, A.J. Bushby, K. Shuturminskaya, M. den Hartog, A. Radaelli, A.H. Negussie, A.S. Mikhail, D.L. Woods, V. Krishnasamy, E.B. Levy, B.J. Wood, S.L. Willis, M.R. Dreher, A.L. Lewis, Characterization of a novel intrinsically radiopaque drug-eluting bead for image-guided therapy: DC Bead LUMITM, *J. Control Release* 250 (2017) 36–47 Mar 28.
- [20] Y.S. Liu, X.Z. Lin, H.M. Tsai, H.W. Tsai, G.C. Chen, S.F. Chen, J.W. Kang, C.M. Chou, C.Y. Chen, Development of biodegradable radiopaque microsphere for arterial embolization-a pig study, *World J. Radiol.* 7 (8) (2015) 212–219 Aug 28.

- [21] Y. Okamoto, T. Hasebe, K. Bito, K. Yano, T. Matsumoto, K. Tomita, A. Hotta, Fabrication of radiopaque drug-eluting beads based on lipiodol/biodegradable-polymer for image-guided transarterial chemoembolization of unresectable hepatocellular carcinoma, *Polym. Degrad. Stab.* 175 (2020) 109106 May.
- [22] A. Poursaid, M.M. Jensen, E. Huo, H. Ghandehari, Polymeric materials for embolic and chemoembolic applications, *J. Control Release* 240 (2016) 414–433 Oct 28.
- [23] A. Jafari, M. Farahani, M. Sedighi, N. Rabiee, H. Savoji, Carrageenans for tissue engineering and regenerative medicine applications: a review, *Carbohydr. Polym.* 281 (2022) 119045 Apr 1.
- [24] S.M. Mihaile, A.K. Gaharwar, R.L. Reis, A.P. Marques, M.E. Gomes, A. Khademhosseini, Photocrosslinkable kappa-carrageenan hydrogels for tissue engineering applications, *Adv. Healthc. Mater.* 2 (6) (2013) 895–907 Jun.
- [25] M.P. Rode, A.B. Batti Angulski, F.A. Gomes, M.M. da Silva, T.D.S. Jeremias, R.G. de Carvalho, D.G. Iucif Vieira, L.F.C. Oliveira, L. Fernandes Maia, A.G. Trentin, L. Hayashi, K.R. de Miranda, A.K. de Aguiar, R.D. Rosa, G.W. Calloni, Carrageenan hydrogel as a scaffold for skin-derived multipotent stromal cells delivery, *J. Biomater. Appl.* 33 (3) (2018) 422–434 Sep.
- [26] S.E. Bakarich, P. Balding, I.I.R. Gorkin, G.M. Spinks, M.I.H. Panhuis, Printed ionic-covalent entanglement hydrogels from carrageenan and an epoxy amine, *RSC Adv.* 4 (72) (2014) 38088–38092 Aug.
- [27] L. Kunliang, J. Zhicheng, H. Xiaolong, Y. Dan, Z. Yu, Z. Haidong, T. Gaojun, X. Fei, A biodegradable multifunctional porous microsphere composed of carrageenan for promoting imageable trans-arterial chemoembolization, *Int. J. Biol. Macromol.* 142 (2020) 866–878 Jan 1.
- [28] G. Gołużki, A. Borowik, A. Lipińska, M. Romanik, N. Derewońska, A. Woziwodzka, J. Piosik, Pentoxifylline affects idarubicin binding to DNA, *Bioorg. Chem.* 65 (2016) 118–125 Apr.
- [29] B. Guiu, G. Hincapie, L. Thompson, Y. Wu, M. Boulin, C. Cassinotto, G.M. Cruise, An *in vitro* evaluation of four types of drug-eluting embolics loaded with idarubicin, *J. Vasc. Interv. Radiol.* 30 (8) (2019) 1303–1309 Aug.
- [30] B. Guiu, P. Chevallier, E. Assenat, E. Barbier, P. Merle, A. Bouvier, J. Dumortier, E. Nguyen-Khac, J. Gugenheim, A. Rode, F. Oberti, P.J. Valette, T. Yzet, O. Chevallier, J.C. Barbare, M. Latournerie, M. Boulin, Idarubicin-loaded beads for chemoembolization of hepatocellular carcinoma: the IDASPHERE II single-arm phase II trial, *Radiology* 291 (3) (2019) 801–808 Jun.
- [31] J. Delicue, B. Guiu, M. Boulin, H. Schwanz, L. Piron, C. Cassinotto, Liver chemoembolization of hepatocellular carcinoma using TANDEM® microspheres, *Future Oncol.* 14 (26) (2018) 2761–2772 Nov.
- [32] V. Verret, J.P. Pelage, M. Wassef, S. Louguet, E. Servais, L. Bédouet, T. Beaulieu, L. Moine, A. Laurent, A novel resorbable embolization microsphere for transient uterine artery occlusion: a comparative study with trisacryl-gelatin microspheres in the sheep model, *J. Vasc. Interv. Radiol.* 25 (11) (2014) 1759–1766 Nov.
- [33] S.I. Jeon, M.S. Kim, H.J. Kim, Y.I. Kim, H.J. Jae, C.H. Ahn, Biodegradable poly(lactide-co-glycolide) microspheres encapsulating hydrophobic contrast agents for transarterial chemoembolization, *J. Biomater. Sci. Polym. Ed.* 33 (4) (2022) 409–425 Mar.
- [34] M.V. Gonzalez, Y. Tang, G.J. Phillips, A.W. Lloyd, B. Hall, P.W. Stratford, A.L. Lewis, Doxorubicin eluting beads-2: methods for evaluating drug elution and in-vitro:in-vivo correlation, *J. Mater. Sci. Mater. Med.* 19 (2) (2008) 767–775 Feb.
- [35] M.J. Song, H.J. Chun, D.S. Song, H.Y. Kim, S.H. Yoo, C.H. Park, S.H. Bae, J.Y. Choi, U.I. Chang, J.M. Yang, H.G. Lee, S.K. Yoon, Comparative study between doxorubicin-eluting beads and conventional transarterial chemoembolization for treatment of hepatocellular carcinoma, *J. Hepatol.* 57 (6) (2012) 1244–1250 Dec.
- [36] M. Boulin, P. Hillon, J.P. Cercueil, F. Bonnetaïn, S. Dabakuyo, A. Minello, J.L. Jouve, C. Lepage, M. Bardou, M. Wendremaire, P. Guérard, A. Denys, A. Grandvilemin, B. Chauffert, L. Bedenne, B. Guiu, Idarubicin-loaded beads for chemoembolisation of hepatocellular carcinoma: results of the IDASPHERE phase I trial, *Aliment Pharmacol. Ther.* 39 (11) (2014) 1301–1313 Jun.
- [37] G.H. Zhou, J. Han, J.H. Sun, Y.L. Zhang, T.Y. Zhou, C.H. Nie, T.Y. Zhu, S.Q. Chen, B.Q. Wang, Z.N. Yu, H.L. Wang, L.M. Chen, W.L. Wang, S.S. Zheng, Efficacy and safety profile of drug-eluting beads transarterial chemoembolization by Calli-Spheres® beads in Chinese hepatocellular carcinoma patients, *BMC Cancer* 18 (1) (2018) 644 Jun 8.
- [38] M. Boulin, A. Schmitt, E. Delhom, J.P. Cercueil, M. Wendremaire, D.C. Imbs, A. Fohlen, F. Panaro, A. Herrero, A. Denys, B. Guiu, Improved stability of lipiodol-drug emulsion for transarterial chemoembolisation of hepatocellular carcinoma results in improved pharmacokinetic profile: proof of concept using idarubicin, *Eur. Radiol.* 26 (2) (2016) 601–609.
- [39] M. Boulin, S. Guiu, B. Chauffert, S. Aho, J.P. Cercueil, F. Ghiringhelli, D. Krause, P. Fagnoni, P. Hillon, L. Bedenne, B. Guiu, Screening of anticancer drugs for chemoembolization of hepatocellular carcinoma, *Anticancer Drugs* 22 (8) (2011) 741–748 Sep.
- [40] G.S. Roth, Y. Teyssier, M. Abousalihiac, A. Seigneurin, J. Ghelfi, C. Sengel, T. Decaens, Idarubicin vs doxorubicin in transarterial chemoembolization of intermediate stage hepatocellular carcinoma, *World J. Gastroenterol.* 26 (3) (2020) 324–334 Jan 21.
- [41] R. Duran, J. Namur, F. Pascale, P. Czuczman, Z. Bascal, H. Kilpatrick, R. Whomsley, S. Ryan, A.L. Lewis, A. Denys, Vandetanib-eluting radiopaque beads: pharmacokinetics, safety, and efficacy in a rabbit model of liver cancer, *Radiology* 293 (3) (2019) 695–703 Dec.
- [42] Y. Qian, Q. Liu, P. Li, Y. Han, J. Zhang, J. Xu, J. Sun, A. Wu, S. Song, W. Lu, Highly tumor-specific and long-acting iodine-131 microbeads for enhanced treatment of hepatocellular carcinoma with low-dose radio-chemoembolization, *ACS Nano* 15 (2) (2021) 2933–2946 Feb 23.
- [43] P.F. Chiang, C.L. Peng, Y.H. Shih, Y.H. Cho, C.S. Yu, Y.M. Kuo, M.J. Shieh, T.Y. Luo, Biodegradable and multifunctional microspheres for treatment of hepatoma through transarterial embolization, *ACS Biomater. Sci. Eng.* 4 (9) (2018) 3425–3433 Sep 10.
- [44] A. Denys, P. Czuczman, D. Grey, Z. Bascal, R. Whomsley, H. Kilpatrick, A.L. Lewis, Vandetanib-eluting radiopaque beads: in vivo pharmacokinetics, safety and toxicity evaluation following swine liver embolization, *Theranostics.* 7 (8) (2017) 2164–2176 Jun 1.
- [45] O.S. Sakr, S. Berndt, G. Carpenter, M. Cuendet, O. Jordan, G. Borchard, Arming embolic beads with anti-VEGF antibodies and controlling their release using Lbl technology, *J. Control Release* 224 (2016) 199–207 Feb 28.
- [46] J.L. Zamorano, P. Lancellotti, D. Rodriguez Muñoz, V. Aboyans, R. Asteggiano, M. Galderisi, G. Habib, D.J. Lenihan, G.Y.H. Lip, A.R. Lyon, T. Lopez Fernandez, D. Mohty, M.F. Piepoli, J. Tamargo, A. Torbicki, T.M. Suter, ESC Scientific Document Group, 2016 ESC position paper on cancer treatments and cardiovascular toxicity developed under the auspices of the ESC committee for practice guidelines: the task force for cancer treatments and cardiovascular toxicity of the European society of cardiology (ESC), *Eur. Heart J.* 37 (36) (2016) 2768–2801 Sep 21.
- [47] R. Lencioni, J.M. Llovet, G. Han, W.Y. Tak, J. Yang, A. Guglielmi, S.W. Paik, M. Reig, D.Y. Kim, G.Y. Chau, A. Luca, L.R. Del Arbol, M.A. Leberre, W. Niu, K. Nicholson, G. Meinhardt, J. Bruix, Sorafenib or placebo plus TACE with doxorubicin-eluting beads for intermediate stage HCC: the SPACE trial, *J. Hepatol.* 64 (5) (2016) 1090–1098 May.
- [48] T. Borde, F. Laage Gaupp, J.F. Geschwind, L.J. Savic, M. Miszcuk, I. Rexha, L. Adam, J.J. Walsh, S. Huber, J.S. Duncan, D.C. Peters, A. Sinusas, T. Schlachter, B. Gebauer, F. Hyder, D. Coman, J.M.M. van Breugel, J. Chapiro, Idarubicin-loaded ONCOZENE drug-eluting bead chemoembolization in a rabbit liver tumor model: investigating safety, therapeutic efficacy, and effects on tumor microenvironment, *J. Vasc. Interv. Radiol.* 31 (10) (2020) 1706–1716 Oct 1.
- [49] S. Favelier, M. Boulin, S. Hamza, J.P. Cercueil, V. Cherblanc, C. Lepage, P. Hillon, B. Chauffert, D. Krausé, B. Guiu, Lipiodol trans-arterial chemoembolization of hepatocellular carcinoma with idarubicin: first experience, *Cardiovasc. Interv. Radiol.* 36 (4) (2013) 1039–1046 Aug.
- [50] B. Guiu, J.L. Jouve, A. Schmitt, A. Minello, F. Bonnetaïn, C. Cassinotto, L. Piron, J.P. Cercueil, R. Loffroy, M. Latournerie, M. Wendremaire, C. Lepage, M. Boulin, Intra-arterial idarubicin-lipiodol without embolisation in hepatocellular carcinoma: the LIDA-B phase I trial, *J. Hepatol.* 68 (6) (2018) 1163–1171 Jun.
- [51] A.B. El-Khoueiry, B. Sangro, T. Yau, T.S. Crocenzi, M. Kudo, C. Hsu, T.Y. Kim, S.P. Choo, J. Trojan, W.T.H. Rd, T. Meyer, Y.K. Kang, W. Yeo, A. Chopra, J. Anderson, C. Dela Cruz, L. Lang, J. Neely, H. Tang, H.B. Dastani, I. Melero, Nivolumab in patients with advanced hepatocellular carcinoma (CheckMate 040): an open-label, non-comparative, phase 1/2 dose escalation and expansion trial, *Lancet* 389 (10088) (2017) 2492–2502 Jun 24.
- [52] S. Qin, Z. Ren, Z. Meng, Z. Chen, X. Chai, J. Xiong, Y. Bai, L. Yang, H. Zhu, W. Fang, X. Lin, X. Chen, E. Li, L. Wang, C. Chen, J. Zou, Camrelizumab in patients with previously treated advanced hepatocellular carcinoma: a multicentre, open-label, parallel-group, randomised, phase 2 trial, *Lancet Oncol.* 21 (4) (2020) 571–580 Apr.
- [53] R.S. Finn, S. Qin, M. Ikeda, P.R. Galle, M. Ducreux, T.Y. Kim, M. Kudo, V. Breder, P. Merle, A.O. Kaseb, D. Li, W. Verret, D.Z. Xu, S. Hernandez, J. Liu, C. Huang, S. Mulla, Y. Wang, H.Y. Lim, A.X. Zhu, A.L. Cheng, IMBrave150 investigators, atezolizumab plus bevacizumab in unresectable hepatocellular carcinoma, *N. Engl. J. Med.* 382 (20) (2020) 1894–1905 May 14.
- [54] R.S. Herbst, J.C. Soria, M. Kowanetz, G.D. Fine, O. Hamid, M.S. Gordon, J.A. Sosman, D.F. McDermott, J.D. Powderly, S.N. Gettinger, H.E. Kohrt, L. Horn, D.P. Lawrence, S. Rost, M. Leabman, Y. Xiao, A. Mokatrin, H. Koeppen, P.S. Hegde, I. Mellman, D.S. Chen, F.S. Hodi, Predictive correlates of response to the anti-PD-L1 antibody MPDL3280A in cancer patients, *Nature* 515 (7528) (2014) 563–567 Nov 27.